V International Conference on Computational Methods in Marine Engineering
MARINE 2013
B. Brinkmann and P. Wriggers (Eds)

SIMULATION OF MOORING CABLE DYNAMICS USING A DISCONTINUOUS GALERKIN METHOD

JOHANNES PALM[⋆], GUILHERME MOURA PAREDES[†], CLAES ESKILSSON[⋆], FRANCISCO TAVEIRA PINTO[†] AND LARS BERGDAHL[⋆]

[⋆] Department of Shipping and Marine Technology
Chalmers University of Technology
SE–412 96 Gothenburg, Sweden
Email: johannes.palm@chalmers.se - Web page: www.chalmers.se

[†] Departamento de Engenharia Civil
Faculdade de Engenharia, Universidade do Porto
Rua Dr. Roberto Frias, s/n, 4200–465 Porto, Portugal
Email: moura.paredes@fe.up.pt - Web page: www.fe.up.pt

Key words: Mooring cable, Discontinuous Galerkin method, High-order finite elements

Abstract. A new numerical model for simulating the dynamics of mooring cables is presented. The model uses the *hp* formulation of the discontinuous Galerkin method. Verification against analytical solutions for a static and a dynamic case is carried out and the model is shown to exhibit exponential convergence with increasing polynomial order of the expansion basis. A simulation of the cyclic movement of a cable endpoint is compared to experimental results, and there is a good agreement between the computed and measured tension force.

1 INTRODUCTION

Snap loads have always been an important aspect of mooring cable dynamics. Within the field of floating wave energy converters (WECs), the importance of snap loads will most likely be even greater. Unlike the typical moored offshore structures, these devices will be installed in relatively shallow water in energetic wave climates. Their working principle of operation in many cases requires them to oscillate at the water surface with large amplitudes and close to their resonant frequency. These characteristics will make the mooring cables of floating WECs more prone to snap load effects, requiring tools that can accurately model this.

Many numerical models for cable dynamics have been proposed since the early 1960's and the work of Walton and Polachek [1]. Some of the more frequently used methods include the finite difference method, e.g.[1, 4], and the popular lumped mass method, e.g.

[2, 3]. Linear finite element methods have been used by e.g. [5] and, more recently, studies employing higher-order finite elements including cubic splines [6] and mixed *hp* elements [7] have been presented.

The formulation presented in this paper uses the discontinuous Galerkin (DG) method of arbitrary spatial order to model a perfectly flexible cable with no bending or torsional stiffness. The hallmark of the DG method is that the solutions are allowed to be discontinuous over elemental boundaries and that the elements are coupled by numerical fluxes, as in the finite volume method. Thus the discrete space of the DG method can be argued to be better suited for handling shock waves such as snap loads. Although the final aim of the new mooring cable solver is directed towards snap loads, in this paper only the first step towards accomplishing this is presented: verification and validation of the fundamental DG model using *hp* elements.

The paper is organised as follows. In Section 2 the equations governing the cable dynamics are presented and in Section 3 the numerical discretization, focusing on the DG method, is described. The results of the numerical model are presented in Section 4. First, to verify the model and to establish the accuracy of the formulation, the model is compared against well known analytical solutions for the static elastic catenary and a linear transverse wave on a string. Then, model simulations of a submerged cable with forced cyclic end point motion are presented and compared to measurements of a physical model test. Finally, concluding remarks are found in Section 5.

2 GOVERNING EQUATIONS

The dynamics of a perfectly flexible cable are described by a one-dimensional second-order non-linear wave equation, see e.g. [5, 7]. Let $\mathbf{r}$ and s denote the cable position vector and the curvilinear abscissa along the unstretched cable, respectively, and let t denote the time. Following [12], the equations are made non-dimensional by scaling $\mathbf{r}$ and s with a characteristic length L_c and by scaling the time with a characteristic time t_c. The cable dynamics in non-dimensional form are then given as

$$\frac{\partial^2 \mathbf{r}}{\partial t^2} - \frac{\partial}{\partial s}\left(c^2 \frac{\partial \mathbf{r}}{\partial s}\right) = \mathbf{f}\,, \tag{1}$$

$$c^2 = \frac{t_c^2}{L_c^2}\frac{EA_0}{\gamma_0}\frac{\epsilon}{1+\epsilon}\,, \tag{2}$$

$$\epsilon = \left|\frac{\partial \mathbf{r}}{\partial s}\right| - 1\,, \tag{3}$$

where c is the non-linear and non-dimensional celerity of the wave propagation and the source term $\mathbf{f}$ represents all external forces acting on the cable segment. In the expression for the celerity, EA_0 and γ_0 are the axial stiffness and mass per unit length of the cable, and ϵ represents the strain. For the typical problems treated in this study the characteristic length of the problem is chosen to be the unstretched length of the cable, and the characteristic time is given by the period of oscillation.

The external forces in $\mathbf{f}$ can be divided into four separate forces: $\mathbf{f} = \mathbf{f}_1 + \mathbf{f}_2 + \mathbf{f}_3 + \mathbf{f_4}$. Here $\mathbf{f}_1$ is the sum of gravity and buoyancy, $\mathbf{f_2}$ is the added mass force, and the tangential and normal drag forces are given as $\mathbf{f}_3$ and $\mathbf{f}_4$. Introducing the unit tangential vector $\mathbf{t}$, defined as

$$\mathbf{t} = \frac{\partial \mathbf{r}}{\partial s} \Big/ \left| \frac{\partial \mathbf{r}}{\partial s} \right| = \frac{\partial \mathbf{r}}{\partial s} \Big/ (1+\epsilon) \ , \tag{4}$$

the expressions for the external forces on the cable segment read

$$\mathbf{f}_1 = -\frac{\gamma_\mathrm{e}}{\gamma_0} \frac{t_c^2}{L_c} \mathbf{g} \, , \tag{5}$$

$$\mathbf{f}_2 = C_\mathrm{M} \frac{A \rho_\mathrm{w}}{\gamma_0} \left(\mathbf{a}_\mathrm{rel} - (\mathbf{a}_\mathrm{rel} \cdot \mathbf{t}) \, \mathbf{t} \right) (1+\epsilon) \ , \tag{6}$$

$$\mathbf{f}_3 = \frac{1}{2} C_\mathrm{Dt} \frac{\rho_\mathrm{w} d L_c}{\gamma_0} \left(\mathbf{v}_\mathrm{rel} \cdot \mathbf{t} \right)^2 \mathbf{t} \, (1+\epsilon) \ , \tag{7}$$

$$\mathbf{f}_4 = \frac{1}{2} C_\mathrm{Dn} \frac{\rho_\mathrm{w} d L_c}{\gamma_0} \left| (\mathbf{v}_\mathrm{rel} - (\mathbf{v}_\mathrm{rel} \cdot \mathbf{t}) \, \mathbf{t}) \right| \left(\mathbf{v}_\mathrm{rel} - (\mathbf{v}_\mathrm{rel} \cdot \mathbf{t}) \, \mathbf{t} \right) (1+\epsilon) \ . \tag{8}$$

Here $\gamma_e = \left((\rho_c - \rho_w) / \rho_c \right) \gamma_0$ is the effective mass per unit length of the submerged cable, ρ_c and ρ_w are the cable and fluid densities. The terms C_M, C_{Dt} and C_{Dn} denote the hydrodynamic coefficients of added mass, tangential drag and normal drag forces, respectively. The last three forces are functions of the relative velocity and relative acceleration of the water with respect to the mooring cable, $\mathbf{v}_\mathrm{rel}$ and $\mathbf{a}_\mathrm{rel}$, given by

$$\mathbf{v}_\mathrm{rel} = \mathbf{v}_\mathrm{w} - \frac{\partial \mathbf{r}}{\partial t} \, , \tag{9}$$

$$\mathbf{a}_\mathrm{rel} = \mathbf{a}_\mathrm{w} - \frac{\partial^2 \mathbf{r}}{\partial t^2} \, . \tag{10}$$

3 NUMERICAL MODEL

3.1 Discontinuous Galerkin method

Let Ω_h denote the partition of the domain Ω into N_{el} elemental domains $\Omega^e = \{ s \,|\, s_l^e \leq s \leq s_u^e \}$ with size boundaries $\partial\Omega^e$ at s_u^e and s_l^e (see Figure 1). The size of the e^{th} element is $h_e = s_u^e - s_l^e$. The first step in the discretization of (1) is to rewrite it as a system of first order differential equations in space, with the use of an auxiliary variable $\mathbf{q}$:

$$\frac{\partial^2 \mathbf{r}}{\partial t^2} = \frac{\partial}{\partial s} \left(c^2 \mathbf{q} \right) + \mathbf{f} \, , \tag{11}$$

$$\mathbf{q} = \frac{\partial \mathbf{r}}{\partial s} \, . \tag{12}$$

Within the e^{th} elemental region the solution, for an arbitrary function f, is approximated by setting $f(s,t) \approx f^e(s,t) = \sum_{i=0}^{i=p} \phi_i(s) \tilde{f}_i^e(t)$. Here $\tilde{f}_i^e(t)$ denotes the local degrees of

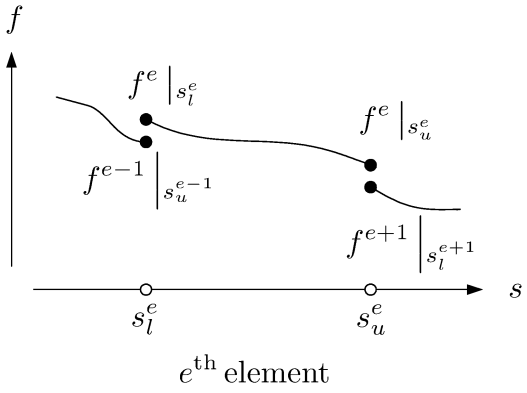

Figure 1: Notation for elemental discretization.

freedom of expansion coefficients and ϕ_i are the expansion basis of order p. In the tests in Section 4 the so-called modal p-type basis [8] is used. This is a hierarchical basis made up of two linear boundary modes and the interior modes given by of Jacobi polynomials.

Taking the inner product $(\cdot\,,\cdot)$ of eqs. (11)–(12) with respect to the basis functions $\phi_k(s)$ we obtain the elemental Galerkin approximation:

$$\left(\phi_k, \frac{\partial^2 \mathbf{r}_h}{\partial t^2}\right)_{\Omega^e} = \left(\phi_k, \frac{\partial}{\partial s}\left(c_h^2 \mathbf{q}_h\right)\right)_{\Omega^e} + (\phi_k, \mathbf{f}_h)_{\Omega^e}\ , \qquad \forall\ k\,, \tag{13}$$

$$(\phi_k, \mathbf{q}_h)_{\Omega^e} = \left(\phi_k, \frac{\partial \mathbf{r}_h}{\partial s}\right)_{\Omega^e}\ . \tag{14}$$

Integrating the terms involving derivatives of s by parts, exchanging the boundary flux terms with numerical fluxes, denoted by $\widehat{\cdot}$, and integrating by parts once more yields the following formulation

$$\left(\phi_k, \frac{\partial^2 \mathbf{r}_h}{\partial t^2}\right)_{\Omega^e} = \left(\phi_k, \frac{\partial}{\partial s}\left(c_h^2 \mathbf{q}_h\right)\right)_{\Omega^e} + \left[\phi_k(\widehat{c_h^2 \mathbf{q}_h}^{\,e} - c_h^2 \mathbf{q}_h^e)\right]_{s_l^e}^{s_u^e} + (\phi_k, \mathbf{f}_h)_{\Omega^e}\ , \tag{15}$$

$$(\phi_k, \mathbf{q}_h)_{\Omega^e} = \left(\phi_k, \frac{\partial \mathbf{r}_h}{\partial s}\right)_{\Omega^e} + [\phi_k(\widehat{\mathbf{r}_h}^{\,e} - \mathbf{r}_h^e)]_{s_l^e}^{s_u^e}\ . \tag{16}$$

For the numerical fluxes, a modified version of the local discontinuous Galerkin (LDG) method developed by Cockburn and Shu [9] is used,

$$\widehat{\mathbf{r}_h} = \{\mathbf{r}_h\} + \beta\,[\mathbf{r}_h]\ , \tag{17}$$

$$\widehat{c_h^2 \mathbf{q}_h} = \{c_h^2 \mathbf{q}_h\} - \beta\left[c_h^2 \mathbf{q}_h\right] + \frac{\eta_1}{h}\,[\mathbf{r}_h] + \eta_2 h\,[\mathbf{v_h}]\ , \tag{18}$$

where η_1 and η_2 are constant mesh-independent parameters, h is the non-dimensional element size, $\beta \in [-1/2, 1/2]$ controls the level of up- and downwinding of the fluxes, and the trace, $\{x\}$, and jump ,$[x]$, operators are introduced as

$$\{x_h^e\}|_s = \frac{1}{2}\left(x_h^e|_{s_u^e} + x_h^{e+1}|_{s_l^{e+1}}\right) \quad \text{if} \quad s = s_u^e\,, \tag{19}$$

$$\{x_h^e\}|_s = \frac{1}{2}\left(x_h^e|_{s_l^e} + x_h^{e-1}|_{s_u^{e-1}}\right) \quad \text{if} \quad s = s_l^e\,, \tag{20}$$

$$[x_h^e]\,|_s = \left(x_h^e|_{s_u^e} - x_h^{e+1}|_{s_l^{e+1}}\right) \quad \text{if} \quad s = s_u^e\,, \tag{21}$$

$$[x_h^e]\,|_s = \left(x_h^{e-1}|_{s_u^{e-1}} - x_h^e|_{s_l^e}\right) \quad \text{if} \quad s = s_l^e\,. \tag{22}$$

The choice of β and η_1 will give rise to different computational stencils affecting the convergence rates [9, 8]. In the test cases presented in Sections 4, $\beta = 0$ is used which gives a centred flux with a wide stencil, but typically allows for larger time steps to be used. The η_1 penalty term is employed to obtain optimal convergence. The use of the additional penalty term η_2, which is non-standard, was found to increase the robustness of the scheme for the validation tests. A more in-depth investigation into the behaviour of the penalty terms is ongoing work.

Dirichlet and Neumann boundary conditions are implemented weakly through the definition of the numerical fluxes [9]

$$\widehat{\mathbf{r}_h} = \mathbf{g}_\mathrm{D} \quad \text{on } \Gamma_\mathrm{D}\,, \qquad \widehat{\mathbf{r}_h} = \mathbf{r}_h^e \quad \text{on } \Gamma_\mathrm{N}\,, \tag{23}$$

$$\widehat{c_h^2\mathbf{q}_h} = (c_h^e)^2\mathbf{q}_h^e + \frac{\eta_1}{h}\left(\mathbf{r}_h^e - \mathbf{g}_\mathrm{D}\right) \quad \text{on } \Gamma_\mathrm{D}\,, \qquad \widehat{c_h^2\mathbf{q}_h} = \mathbf{g}_\mathrm{N} \quad \text{on } \Gamma_\mathrm{N}\,, \tag{24}$$

where $\mathbf{g}_\mathrm{D}$ and $\mathbf{g}_\mathrm{N}$ are the non-dimensionalised values at the cable end points.

3.2 Time-stepping scheme

Presently the numerical model uses explicit time-stepping schemes, either the third-order Runge-Kutta scheme [9] typically associated with DG schemes or a simple second-order central differencing scheme. The computations presented in this paper have used the central differencing scheme. Writing the semi-discrete equations as

$$\frac{\partial^2 \mathbf{r}_h}{\partial t^2} = \mathbf{L}_h\left(\mathbf{r}_h\right)\,, \tag{25}$$

advancing from time level n to $n+1$ for the central differencing scheme is simply

$$\mathbf{r}_h^{n+1} = 2\mathbf{r}_h^n - \mathbf{r}_h^{n-1} + \Delta t^2 \mathbf{L}_h\left(\mathbf{r}_h\right)\,. \tag{26}$$

It should be noted that the time step restriction for explicit schemes for second-order spatial derivatives is very restrictive as $\Delta t \propto p^{-4}$ [8]. Thus implicit schemes will be considered in later studies.

4 TEST CASES

The convergence of the model and the quality of the simulation results are verified by comparison with analytical solutions for known cases. The error in the L_2-norm of the results is computed for different choices of polynomial order p and element size h. The L_2 error is defined as

$$\|f\|_{L_2} = \sqrt{\int_\Omega (f_{exact} - f)^2 \, \mathrm{d}\Omega}\,, \tag{27}$$

and is evaluated using the quadrature points inside every element e.

4.1 Static verification - elastic catenary equation

The analytical solution to the static equilibrium of an elastic catenary can be found in e.g. [10] and is well known:

$$x = a_\mathrm{T} \mathrm{sinh}^{-1}\left(\frac{s}{a_\mathrm{T}}\right) + a_\mathrm{T}\frac{\gamma_\mathrm{e} g}{EA_0} s\,, \tag{28}$$

$$z = \sqrt{a_\mathrm{T}^2 + s^2} + \frac{\gamma_\mathrm{e} g}{2EA_0} s^2 - a_\mathrm{T}\,, \tag{29}$$

$$a_\mathrm{T} = \frac{T_\mathrm{H}}{\gamma_\mathrm{e} g}\,. \tag{30}$$

The horizontal component of the tension force, T_H, is constant along the cable and the origin of the x, z and s coordinates is the lowest point of the catenary. The equations are implicit when T_H is unknown, and are solved numerically for each set of cable conditions.

The computed cable has a stiffness of $EA_0 = 200$ kN/m, a mass of $\gamma_e = 1.738$ kg/m and an unstretched length L of 100.5 m. The attachment points of the cable are horizontally aligned and distanced by 100 m. Three cases are examined:

- p-type refinement ($N_{el} = 2$ with $p = 1\,, \ldots\,, 9$),
- h-type refinement using linear elements ($N_{el} = 1\,, 2\,, 4\,, \ldots\,, 20$ with $p = 1$),
- h-type refinement using quadratic elements ($N_{el} = 1\,, 2\,, 4\,, \ldots\,, 20$ with $p = 2$).

The computational results in terms of L_2 error of the cable position versus total degrees of freedom are presented in Figure 2. Both the expected exponential convergence of the p-type refinement (as illustrated by the straight line for $h = 2$ in the semi-log plot to the left in Figure 2) and the algebraic convergence of the h-type refinement (as demonstrated by the straight lines in the logarithmic plot to the right of Figure 2) are shown in the result. The benefit in using high-order methods for smooth problems in terms of accuracy per degree of freedom is obvious.

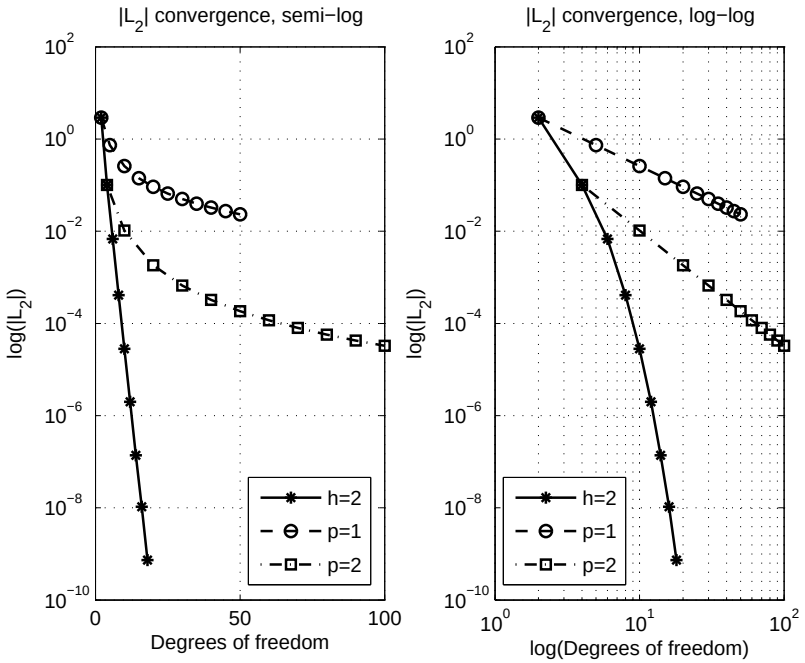

Figure 2: L_2 error of the cable position as a function of the total number of degrees of freedom for the elastic catenary case.

4.2 Dynamic verification - standing wave on a taut cable

Consider a cable with constant tension and strain, no external forces applied and only transverse displacements allowed. Then eq. (1) simplifies to the standard linear wave equation

$$\frac{\mathrm{d}^2 r}{\mathrm{d}t^2} = \frac{T}{\gamma_0(1+\epsilon)} \frac{\partial^2 r}{\partial s^2} \,. \tag{31}$$

The term $T/\left(\gamma_0(1+\epsilon)\right)$ in eq. (31) is the square of the celerity of the wave in the unstretched computational domain s. The celerity of the wave in the physical domain is

$$c_p = \sqrt{\frac{T}{\gamma_\mathrm{p}}} = \sqrt{\frac{T(1+\epsilon)}{\gamma_0}} \,, \tag{32}$$

where γ_p is the mass per unit length of the stretched cable. Let the end points of the cable be horizontally aligned and stretch it to form a half sine arch that is centred at the midpoint of the cable. The analytical solution to this problem then reads [11]:

$$y(x,t) = A\cos\left(c_p \frac{\pi}{L(1+\epsilon)} t\right) \sin\left(\frac{\pi}{L(1+\epsilon)} x\right) \,, \tag{33}$$

where A is the maximum amplitude of the displacement.

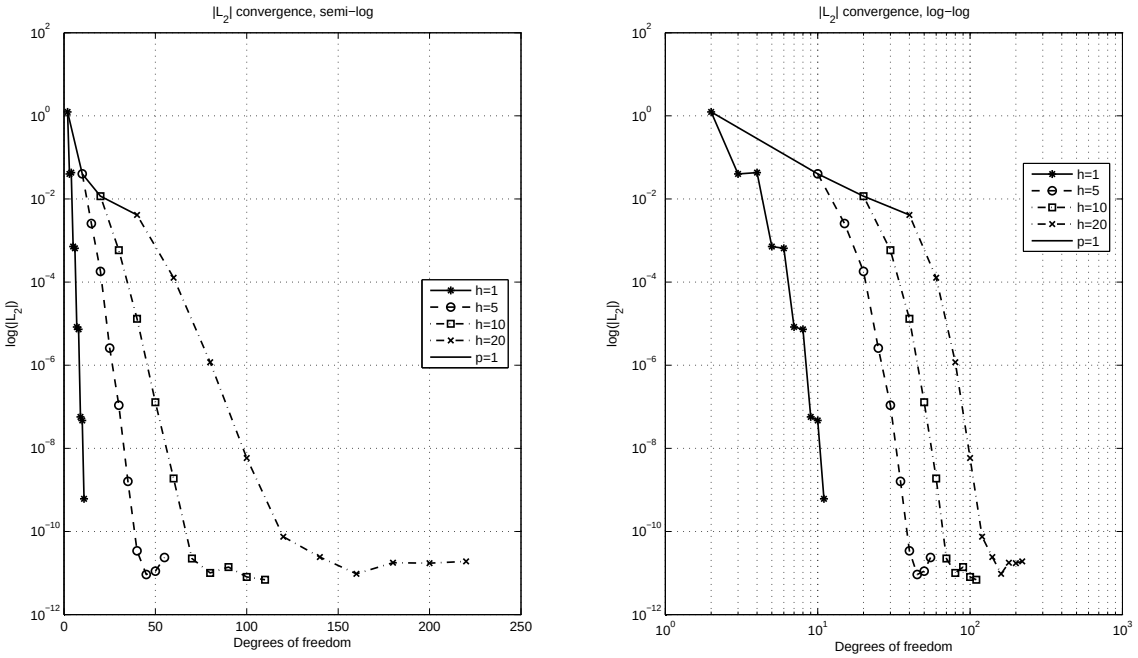

Figure 3: L_2 error of the cable position as a function of the total number of degrees of freedom for the elastic standing wave case.

The computed cable has a constant tension $T = 1\,\mathrm{N}$, a mass of $\gamma_0 = 1\,\mathrm{kg/m}$ and an unstretched length L of $0.5\,\mathrm{m}$. The attachment points are distanced by $1\,\mathrm{m}$ and the wave amplitude is set to $1\,\mathrm{m}$. The domain is divided into $N_{el} = 1\,, 5\,, 10\,, 20$ elements with $p = 1\,, \ldots\,, 10$. For this case no penalty term is used in the model. The solution is integrated for $2\,\mathrm{s}$ (one complete oscillation cycle) using a sufficiently small time step to ensure spatial errors dominate.

The computational results in terms of L_2 error of the cable position versus total degrees of freedom are presented in Figure 3. It is shown that – as for the static catenary case – p-type refinement yields exponential convergence until the error get saturated around machine precision ($\approx 1 \times 10^{-12}$ for the present case). It should be mentioned that the convergence rates are generally sub-optimal and of order p. This is as expected since centred numerical fluxes without penalty terms is known to loose an order of convergence [9].

4.3 Validation test - comparison against the experiments of Lindahl

The model test of Lindahl [12] is used for validating the dynamic behaviour of the cable solver against experimental measurements. In this section, the measured cable top end force results will be compared to those computed by the numerical model.

The experimental set-up is shown in Figure 4. The experimental measurements were

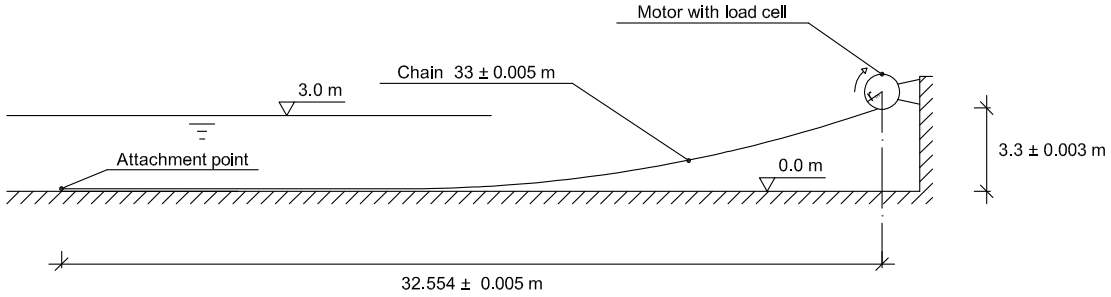

Figure 4: The geometrical setup of the experimental tests by [12].

made on a 33m steel chain ($\rho_c = 7800$ kg/m^3) submerged in 3m of water ($\rho_w = 1000$ kg/m^3). One end was attached to the concrete floor and the other end was attached to a circular plate with a fixed rotation speed. The radius of motion in the cases compared in this study was 0.2 m. The cable characteristics suggested in [12] are presented in Table 1.

In the experiments the top part of the chain was suspended in air and the rest was submerged in water. This is taken into account in the numerical model by the use of the dry weight for the gravity force and by excluding any added mass- or drag forces acting on the cable segment above the height of 3 m.

The interaction between cable segments and the concrete floor is handled by a ground interaction model made up of a bilinear spring and damper system in the normal (vertical) direction and a dynamic friction in the tangential direction [13, 3]. The characteristics of the ground model are presented in Table 1. Please note that $G_{\mathrm{v_c}} = 0.01$ m/s is the velocity at which the dynamic, tangential friction force reaches its maximum value. Up to that value, the friction force is ramped up from 0. The forces acting on the cable when it is interacting with the ground are given by:

$$\mathbf{F}_{\mathrm{Gz}} = -G_{\mathrm{K}}\, d\, \Delta z - 2\, G_{\mathrm{C}} \sqrt{\frac{G_K d}{\gamma_0}}\, \min\left(0\,, v_z\right) + \gamma_e\, g\,, \tag{34}$$

$$\mathbf{F}_{\mathrm{Gxy}} = -\gamma_{\mathrm{e}}\, g\, G_\mu \min\left(\frac{v_{\mathrm{xy}}}{G_{\mathrm{v_c}}}, 1\right)\,, \tag{35}$$

where $\Delta z \geq 0$ is the ground penetration depth, v_z is the vertical velocity of the cable and $v_{\mathrm{xy}} = \sqrt{v_{\mathrm{x}}^2 + v_{\mathrm{y}}^2}$ is the velocity of the cable tangential to the ground.

In the computations the cable is divided into 10 elements with polynomial order $p = 7$. Two cases with rotational periods of $T_r = 3.5$ s and $T_r = 1.25$ s, respectively, are investigated. The simulations are integrated in time for 15 rotational periods. The resulting forces in the top end are shown in Figures 5 and 6.

As seen in Figures 5 and 6 the values match very well. The maximum value of the tension force is correct within a few percent, and the high frequency oscillations that

Table 1: Characteristics of the cable and the ground interaction model used in the Lindahl cases.

Name	Value	Unit	Description
L	33	m	Cable length
γ_0	0.018	kg/m	Mass per length
EA_0	10000	N	Cable stiffness
d	0.002	m	Nominal cable diameter
C_{Dt}	0.5	-	Tangential drag coefficient
C_{Dn}	2.5	-	Normal drag coefficient
C_{M}	3.8	-	Added mass coefficient
G_{K}	3	GPa/m	Ground normal stiffness per unit area
G_{C}	1	-	Fraction of critical damping of ground
G_{μ}	0.3	-	Friction coefficient
$G_{\mathrm{v_c}}$	0.01	m/s	Cut-off velocity of friction

appear for very low tension force magnitude are small in amplitude. The end force is never completely slack for the $T_r = 3.5$ s case, however other parts of the cable has tension force that vanishes completely. In the more high frequency case of $T_r = 1.25$ s the end point force does however vanish completely. As the entire cable looses stiffness at some instances in time, the numerical oscillations after the slack are larger in the case of higher frequency of excitation. These numerical oscillations are quickly damped out as the cable tension increases, and the inaccuracy is only evident for very low tension force magnitudes. The computed maximum force however is still in excellent agreement with the experimental data. It is worth to point out that the results presented here are unfiltered and have not been smoothed in any way. It should also be mentioned that the ground interaction model has a large influence on the solutions and that further studies into the effect of the ground model for high-order solutions are required.

5 CONCLUDING REMARKS

The presented high-order DG formulation for the solution of cable dynamics shows good agreement with both experimental and analytical data, confirming the accuracy of the model formulation. The model is shown to exhibit the expected exponential convergence associated with p-type refinement. The DG approach allows for discontinuities in the solution – often appearing due to the cable becoming slack, as seen in the Lindahl cases. However, Gibbs-type oscillations, typically associated with the use of high-order schemes in the presence of discontinuities, are occurring in the absence of any artificial viscosity, limiters or filters. In the Lindahl cases stability of the solutions is obtained through the use of the penalty terms. Optimising the penalty terms as well as adding additional shock-capturing capabilities in order to better handle snap loads is ongoing work.

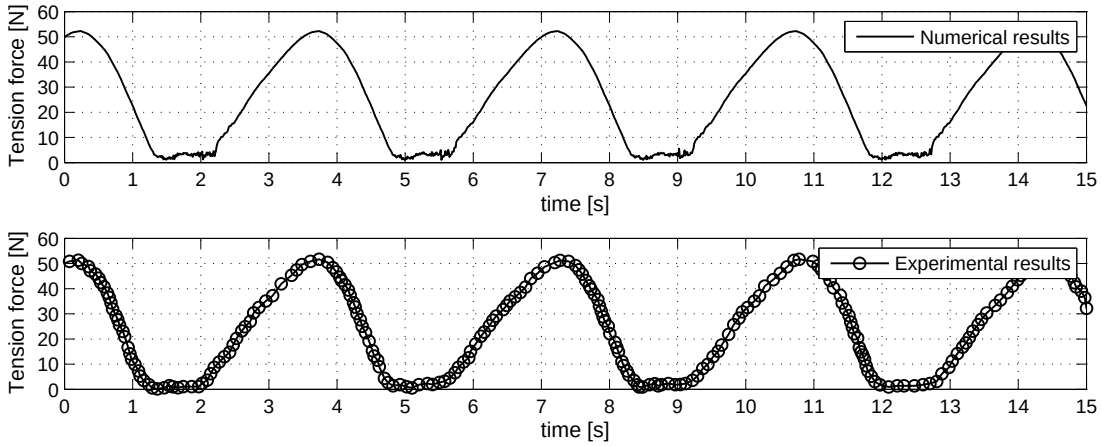

Figure 5: Comparison between the experimental and numerical cable top end forces. $r = 0.2\,\mathrm{m}$ and $T_r = 3.5\,\mathrm{s}$.

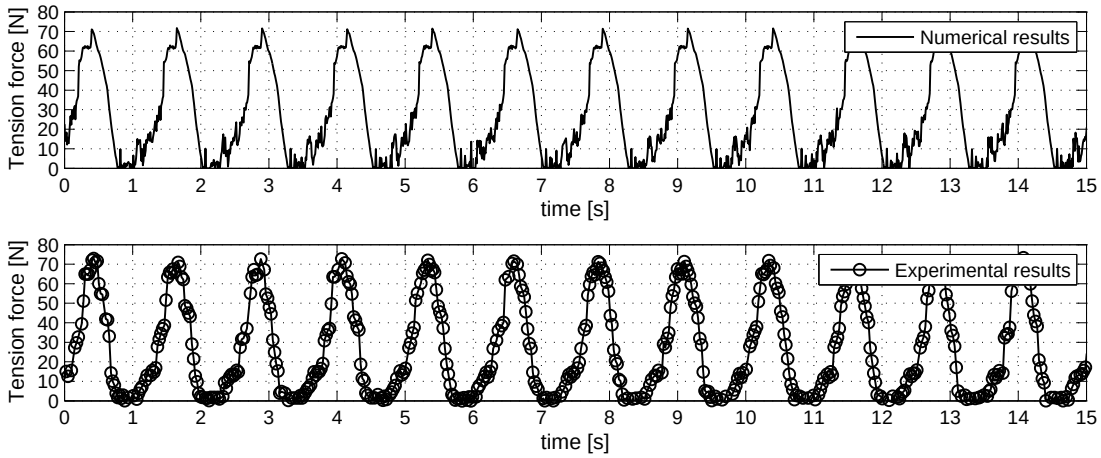

Figure 6: Comparison between the experimental and numerical cable top end forces. $r = 0.2\,\mathrm{m}$ and $T_r = 1.25\,\mathrm{s}$.

ACKNOWLEDGEMENTS

This work was funded by the Swedish collaboration platform Ocean Energy Centre (hosted by Chalmers University of Technology and supported by a grant from Region Västra Götaland, the regional development agency of Västra Götaland in Western Sweden) and by the Portuguese Foundation for Science and Technology (FCT – Fundação para a Ciência e Tecnologia) through research grant SFRH/BD/62040/2009.

REFERENCES

[1] Walton, T.S. and Polachek, H. Calculation of transient motion of submerged cables. *Math. Comp.* (1969) **14**:27–46 .

[2] Khan, N.U. and Ansari, K.A. On the dynamics of a multicomponent mooring line. *Comp. Struc.* (1986) **22**:311–334.

[3] Orcina Ltd. *OrcaFlex manual – version 9.5a.* (2012).

[4] Roussel, P. Numerical solution of static and dynamic equations of cables. *Comp. Meth. Appl. Mech. Engng.* (1976) **9**:65–74.

[5] Aamo, O.M. and Fossen, T.I. Finite element modelling of mooring lines. *Math. Comp. Sim.* (2000) **53**:415–422.

[6] Escalante, M.R., Sampaio, R., Rosales, M.B. and Ritto, T. A reduced order model of a 3D cable using proper orthogonal decomposition. *Mec. Comp.* (2011) **XXX**:1143–1158.

[7] Montano, A. and Restelli, M. and Sacco, R. Numerical simulation of tethered buoy dynamics using mixed finite elements. *Comp. Meth. Appl. Mech. Engng.* (2007) **196**:4117–4129.

[8] Karniadakis, G.Em. and Sherwin, S.J. *Spectral/hp element methods for CFD.* Oxford University Press, 2nd edition, (2003).

[9] Cockburn, B. and Shu, C.-W. Runge-Kutta discontinuous Galerkin methods for convection-dominated problems. *J. Sci. Comp.* (2001) **16**:173–261.

[10] Sjöberg, A. and Bergdahl, L. *Förankringar och förankringskrafter.* Report Series B:30, Department of Hydraulics, Chalmers University of Technology, (1981).

[11] Greiner, W. *Classical mechanics: systems of particles and Hamiltonian dynamics.* Springer, (2003).

[12] Lindahl, J. *Modellförsök med en förankringskabel.* Report Series A:12, Department of Hydraulics, Chalmers University of Technology, (1985).

[13] Lindahl, J. *Implicit numerisk lösning av rörelseekvationerna för en förankringskabel.* Report Series A:11, Department of Hydraulics, Chalmers University of Technology (1984).